Supporting Information

The Role of Protons and Hydrides in the Catalytic Hydrogenolysis of Guaiacol at the Ruthenium Nanoparticle-water Interface

Junnan Shangguan,[‡] Alyssa J.R. Hensley, [^,‡,] Matthew V. Gradiski,[§] Niklas Pfriem,[‡] Jean-Sabin McEwen, [^, ǁ, #, &, †] Robert H. Morris,[§] Ya-Huei (Cathy) Chin[‡*]

[‡]Department of Chemical Engineering and Applied Chemistry, University of Toronto, Toronto, M5S 3E5, Canada;

[§]Department of Chemistry, University of Toronto, Toronto, M5S 3H6, Canada;

[^] The Gene & Linda Voiland School of Chemical Engineering and Bioengineering, Washington State University, Pullman, WA 99164, United States;

[ǁ]Institute for Integrated Catalysis, Pacific Northwest National Laboratory, Richland, WA, 99352, United States;

[#]Department of Physics and Astronomy, Washington State University, Pullman, WA 99164, United States;

[&]Department of Chemistry, Washington State University, Pullman, WA 99164, United States;

[†]Department of Biological Systems Engineering, Washington State University, Pullman, WA 99164, United States;

Corresponding author email address: cathy.chin@utoronto.ca

S1. Ruling out significant H/D exchange on the methyl group of guaiacol by mass spectroscopy analyses

Figure S1 shows that the molar fractions of deuterated guaiacol, derived from the base ion that has a total number of x deuterium atoms on its aromatic ring and hydroxyl group (m/z = 109 + x, x = 0-5), increase linearly with a slope of unity with the molar fractions of deuterated guaiacol, derived from the molecular ion that has a total number of y deuterium atoms on its aromatic ring, hydroxyl group, and methyl group (m/z = 124 + y, y = 0-5) for all time-dependent molar fractions during (a) **I** (4.1×10^{-2} M)-D_2O reaction in He without Ru catalyst (Figure S1a), (b) **I** (4.1×10^{-2} M)-D_2O reaction in He with 50 mg 1 wt.% Ru/C (Figure S1b), and (c) [4,6-D_2]-**I** (3.3×10^{-2} M)-D_2O reactions with 50 mg 1 wt.% Ru/C at one atmospheric pressure of D_2 (balanced with 10 bar He at 298 K, Figure S1c). These linear dependences between base ions and molecular ions under all three reactions and over the entire molar fraction ranges, indicate that the H/D isotopic exchange does not occur on methyl group [C(-7)H_3], which is consistent with previous findings reported for guaiacol (4.3×10^{-2} M)-H_2 (30 bar)-D_2O reaction on 14 nm 1 wt.% Ru/C at 423 K.[1] These results led us to rule out any significant H/D isotopic exchange on the methyl group [C(-7)H_3] during homogeneous and heterogeneous H/D exchange reactions.

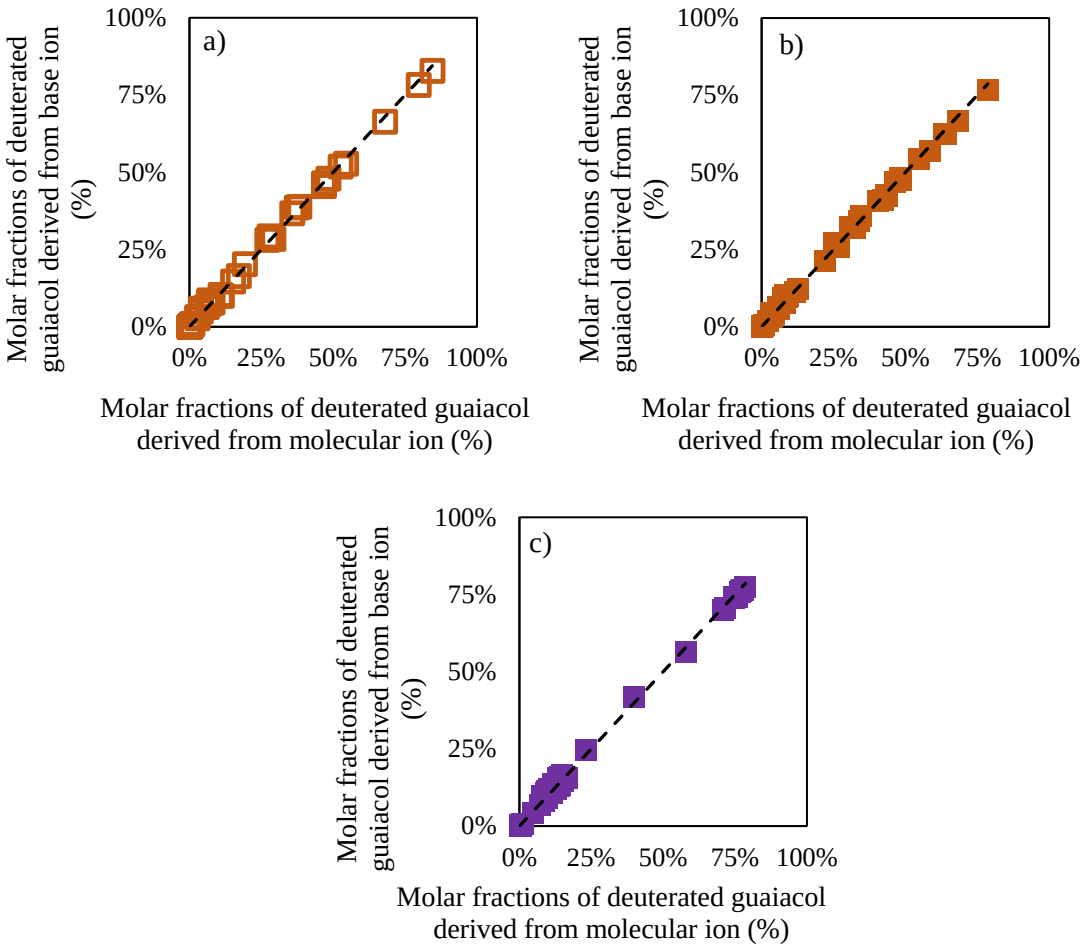

Figure S1. Molar fractions of guaiacol with *x* number of deuterium derived from base ion (mass-to-charge ratio, m/z = 109 + *x*, *x* = 0-5) as a function of the corresponding molar fractions of guaiacol with *y* number of deuterium derived from molecular ion (m/z = 124 + *y*, *y* = 0-5) during a) guaiacol [$C_6H_4(OCH_3)(OH)$, 4.1 × 10^{-2} M]-D_2O reactions without a catalyst (□), b) guaiacol [$C_6H_4(OCH_3)(OH)$, 4.1 × 10^{-2} M]-D_2O reactions with 50 mg 1 wt.% Ru/C (14 nm mean Ru cluster size, ■), and c) [4,6-D_2]-**I** (3.3 × 10^{-2} M)-D_2O reactions with 50 mg 1 wt.% Ru/C (14 nm mean Ru cluster size) in atmospheric pressure of D_2 (balanced with 10 bar He at 298 K, ■) at 423 K. Dotted lines are linear trend lines with their slopes equal unity.

S2. ^{1}H and ^{13}C-NMR assignments of guaiacol in D_2O

The assignment starts with determining the chemical shift of the methoxy (OMe) substituent. This is done using a phase-shifted (PS) HSQC NMR experiment as shown in Figure S2. The ^{1}H shift of the methyl protons at 3.89 ppm is much further upfield than the aromatic protons (in the region 6.5-8.0 ppm) and is a trivial assignment, as is the methoxy carbon atom C-7 at 55.8 ppm correlated with these methyl protons. Note that in D_2O, the OH resonance will be completely converted to OD with some HDO produced.

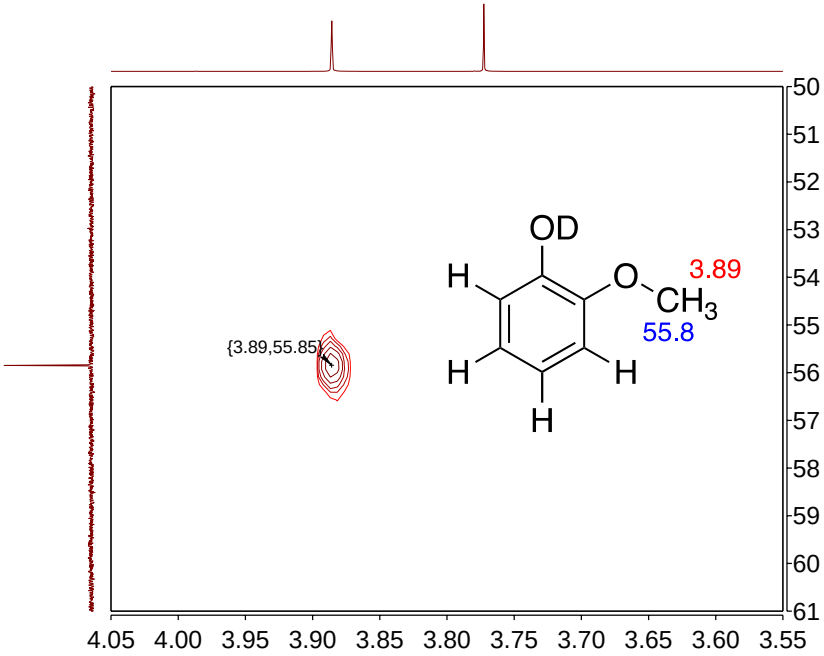

Figure S2. A section of the PS-HSQC NMR spectrum of guaiacol in D_2O that is used to identify the ^{1}H and ^{13}C chemical shifts of the OC(-7)H_3 group of guaiacol. The ^{1}H spectrum in the range of 4.05 to 3.55 ppm is plotted along the *x* axis with resonances assigned to the CH_3 resonance at 3.89 ppm and a dioxane reference peak at 3.77 ppm and the $^{13}C\{^{1}H\}$ spectrum in the range 61 to 51 ppm, along the *y* axis with the C-7 peak at 55.8 ppm.

Next, to determine the carbon assignments of atoms bonded to oxygen, an HMBC NMR experiment (Figure S3) is conducted. A three-bond ^{13}C(-2)-O-C(-7)-^{1}H correlation is observed between the aromatic carbon C-2, which is assigned to the peak at 147 ppm and bonded to the methoxy OC(-7)H_3 substituent, with the ^{1}H resonance at 3.89 ppm as assigned above. A three-bond ^{13}C(-2)-O-C(-7)-^{1}H correlation is observed between the aromatic carbon C-2 assigned to the peak at 147 ppm bonded to the methoxy OC(-7)H_3 substituent with the ^{1}H resonance at 3.89 ppm as assigned above. By exclusion, the other ^{13}C resonance present above 140 ppm

must be the aromatic C-1 atom at 144 ppm that is bonded to the OD substituent.

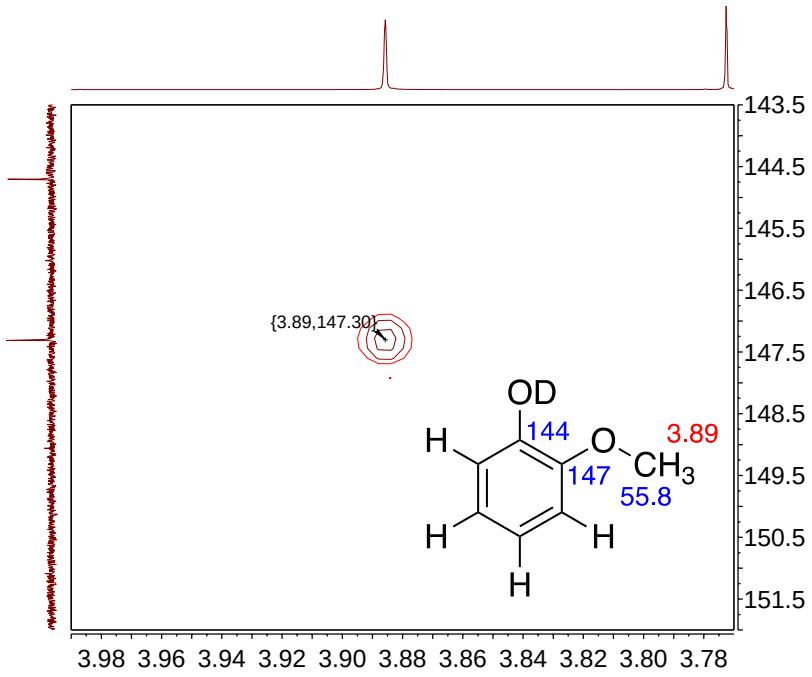

Figure S3. HMBC NMR spectrum of guaiacol used to determine the assignment of the ^{13}C resonances with chemical shifts greater than 140 ppm. The section plotted shows the ^{1}H spectrum in the range of 3.99 to 3.77 ppm along the *x* axis with the CH_3 resonance at 3.89 ppm and the dioxane reference peak at 3.77 ppm and the $^{13}C\{^{1}H\}$ spectrum in the range 152 to 143.5 ppm, along the *y* axis with C-2 at 147 ppm and C-1 at 144 pm. No ^{13}C NMR peaks are observed above 152 ppm.

Subsequently, we determine the chemical shift of the proton on carbon atom C-3 through ^{1}H-^{1}H COSY. A five-bond ^{1}H-^{13}C(-3)-^{13}C(-2)-O-^{13}C(-7)-^{1}H correlation is observed between the proton on carbon atom C-3 at 7.09 ppm and the methyl protons on carbon atom C-7, as shown in Figure S4.

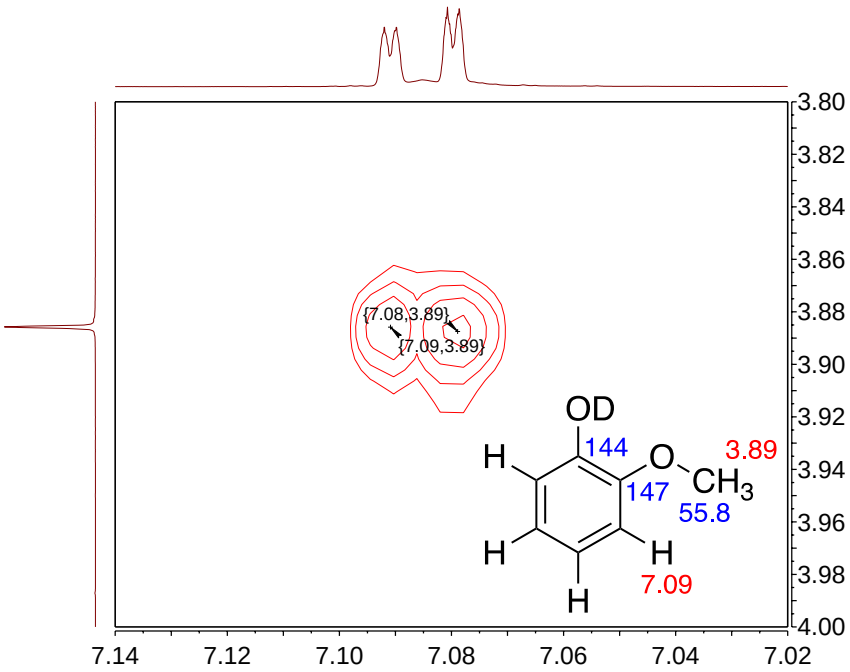

Figure S4. ^{1}H-^{1}H COSY NMR spectrum of guaiacol used to determine the assignment of the proton resonance on carbon atom C-3. The section plotted shows the ^{1}H spectrum in the range of 7.14 to 7.02 ppm along the *x* axis with the CH resonance at 7.08 ppm and the ^{1}H spectrum in the range 4.00 to 3.80 ppm along the *y* axis with the CH_3 resonance at 3.89 ppm.

With the resonance of the proton on carbon atom C-3 now known, a band-selective ^{1}H-^{13}C HSQC is conducted to determine the chemical shift of the carbon atom in position C-3 as 112 ppm shown in Figure S5 as a one bond ^{1}H-^{13}C-3 correlation.

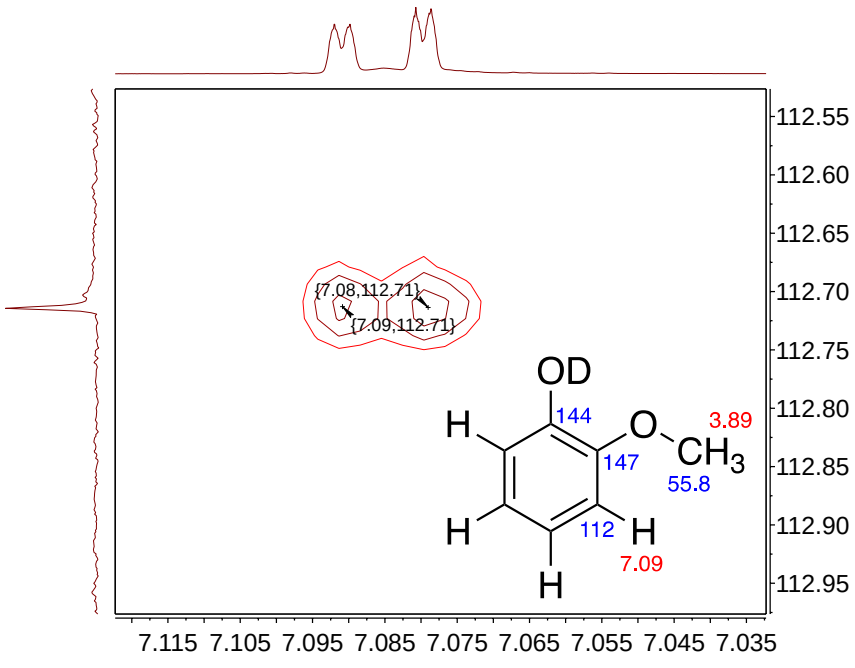

Figure S5. Band-selective ^{1}H-^{13}C HSQC spectrum of guaiacol used to determine the assignment of the resonance of carbon atom C-3. The section plotted shows the ^{1}H spectrum in the range of 7.115 to 7.035 ppm on the *x* axis with the CH resonance of carbon atom C-3 at 7.08 ppm and the $^{13}C\{^{1}H\}$ spectrum in the range of 112.95 to 112.55 ppm on the *y* axis with C-3 at 112.71 ppm.

With the resonances of the proton and carbon atom in position C-3 known, the proton and carbon resonances of position C-6 can be determined by exclusion as it is the only remaining position with a ^{13}C resonance below 120 ppm and is assigned as 115 ppm via a ^{1}H-^{13}C PS-HSQC. Carbon atoms in positions C-4 and C-5 will have resonances downfield of positions C-3 and C-6 due to the para influence from oxygen bound carbon atoms. Again, using PS-HSQC, the chemical shift of the proton in position C-6 can be determined and is assigned as 6.97 ppm, shown in Figure S6. This NMR spectrum also reveals the proton and carbon resonances of positions C-4 and C-5 that can be assigned using ^{1}H-^{13}C HMBC in Figure S7. The HMBC spectrum shows two distinct 3-bond correlations. The first between the C-3 proton at 7.09 ppm and the C-5 carbon atom assigned as 121.6 ppm [^{1}H-^{13}C(-3)-^{13}C(-4)-^{13}C(-5)]. The other is between the C-6 proton at 6.97 ppm and the C-4 carbon atom assigned as 121 ppm [^{1}H-^{13}C(-6)-^{13}C(-5)-^{13}C(-4)].

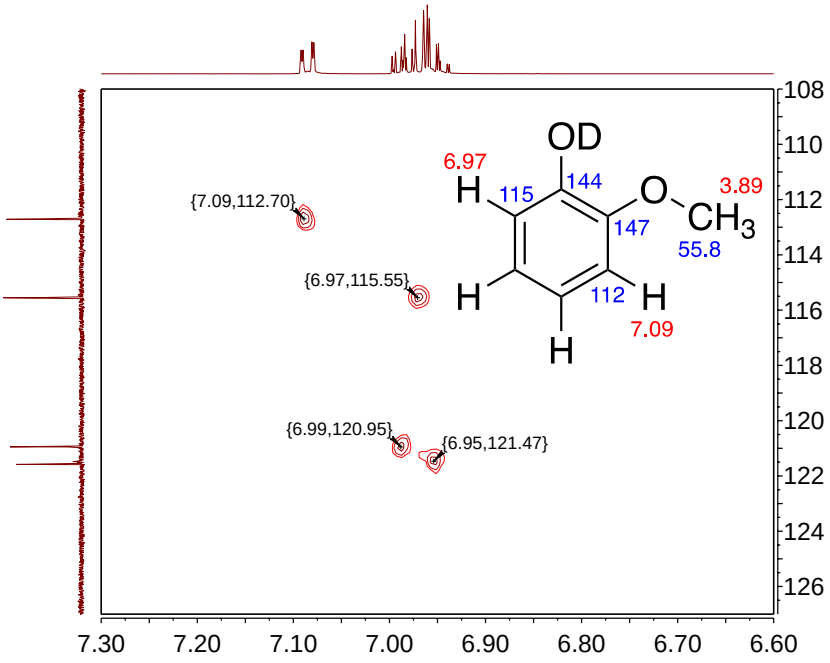

Figure 6. ^{1}H-^{13}C PS-HSQC spectrum of guaiacol used to determine the resonance of the carbon atom in position C-6 and resonances of carbon atoms in positions C-4 and C-5. The section plotted shows the ^{1}H spectrum in the range 7.30 to 6.60 ppm on the *x* axis with the CH resonance of carbon atom C-6 at 6.97 ppm and $^{13}C\{^{1}H\}$ spectrum in the range 127 to 108 ppm on the *y* axis with the carbon resonance of carbon atom C-

6 at 115 ppm.

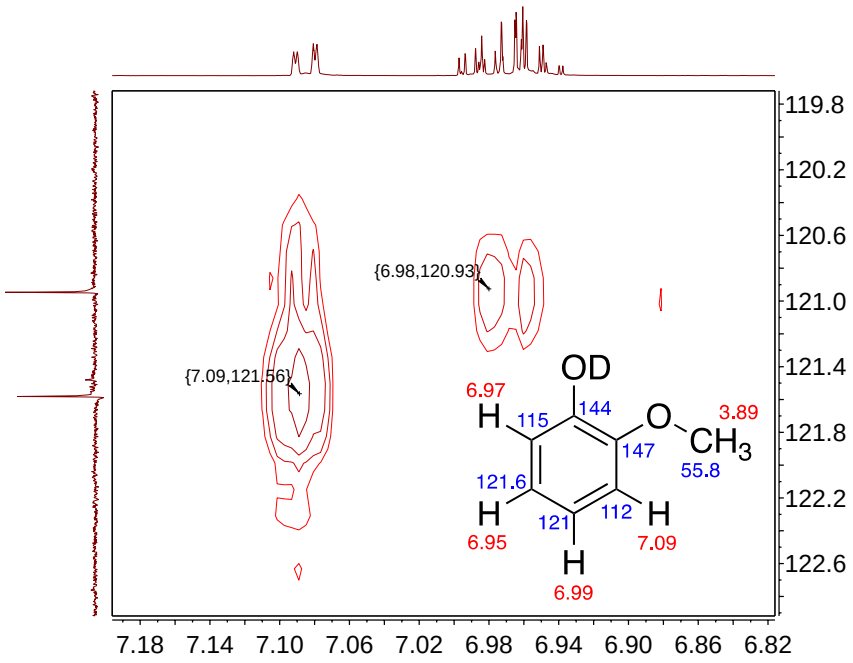

Figure S7. ^{1}H-^{13}C HMBC spectrum of guaiacol used to determine the resonances of carbon atoms in positions C-4 and C-5. The section plotted shows the ^{1}H spectrum in the range 7.19 to 6.82 ppm on the *x* axis with the CH resonance of carbon atom C-6 at 6.98 ppm and the CH resonance of carbon atom C-3 at 7.09 ppm respectively. The ^{13}C spectrum in the range 122.8 to 119.8 ppm on the *y* axis with carbon resonance of carbon atom C-4 at 120.93 (121) ppm and resonance of carbon atom C-5 at 121.56 (121.6) ppm respectively.

To further confirm the assignments of the protons on carbon atoms C-3 and C-5, we characterize the synthesized [4,6]-D_2-**I** sample using qNMR in Figure S8. It shows a 1:1 integration of both remaining protons on carbon atoms C-3 and C-5. The integration is relative to the methoxy protons on carbon atom C-7, since H/D exchange does not occur on C-7, Section S1.

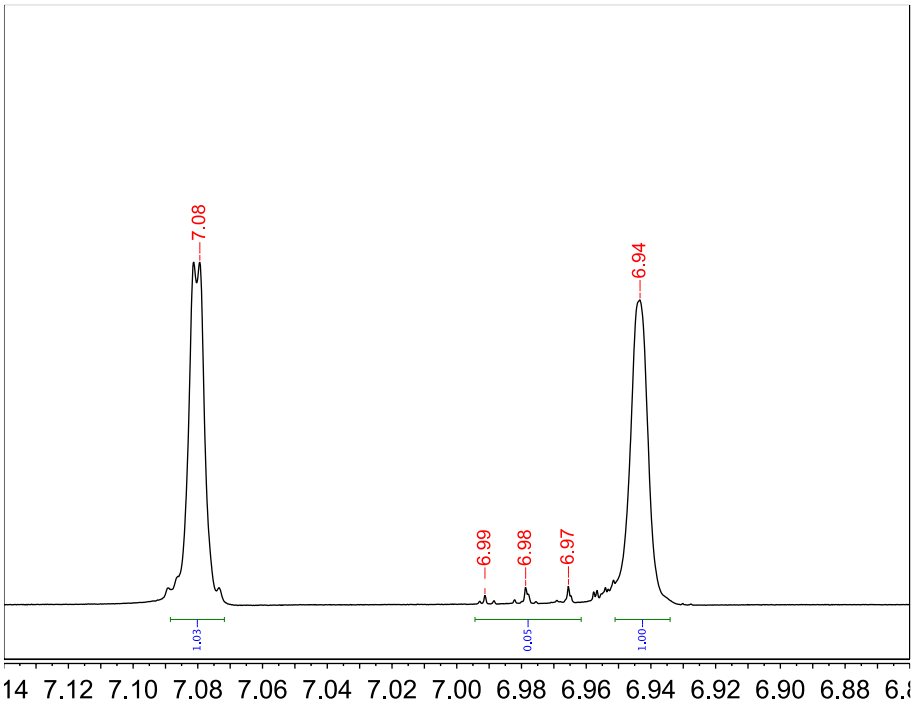

Figure S8. ^{1}H qNMR spectrum of synthesized [4,6-D_2]-**I** [3.3 × 10^{-2} M] sample (in D_2O, air, measured at 298 K); the integrations are relative to protons on C-7.

Figure S9 shows the ^{1}H-^{1}H COSY spectrum of the same sample of [4,6-D_2]-**I** as in Figure S8. The full spectrum is shown in Figure S10. There are no observed three-bond correlations between protons on C-3/C-4, C-4/C-5, or C-5/C-6 because positions C-4 and C-6 have been exchanged with ^{2}H (or denoted as D). The major correlation that is observed is between the two remaining protons on positions C-3 and C-5, a four-bond ^{1}H-C(-3)-C(-4)-C(-5)-^{1}H correlation as shown in Figure S9. We assigned the proton on carbon atom C-3 at 7.09 ppm and the evidence for this was a five-bond COSY correlation between the C-3 proton and the C-7 methoxy group as shown in Figure S4. The five-bond correlation between the C-3 proton and C-7 methoxy group is still observed in this sample as shown in Figure S10. Additionally, a 2D-NOESY spectrum reveals a NOE through-space interaction between protons in the C-3 position and C-7 position as shown in Figure S11.

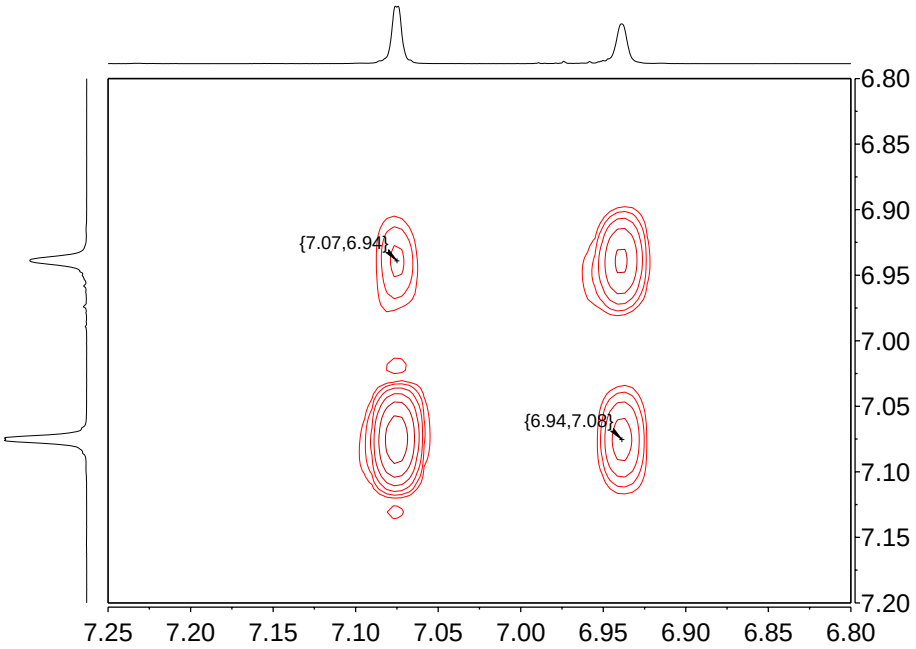

Figure S9. ^{1}H-^{1}H COSY of synthesized [4,6-D_2]-**I** [3.3 × 10^{-2} M] sample showing a four-bond ^{1}H-C(-3)-C(-4)-C(-5)-^{1}H correlation between protons in position C-3 and C-5. The section plotted shows the ^{1}H spectrum in the range 7.25 to 6.80 ppm on the *x* axis and ^{1}H spectrum in the range 7.20 to 6.80 ppm on the *y* axis.

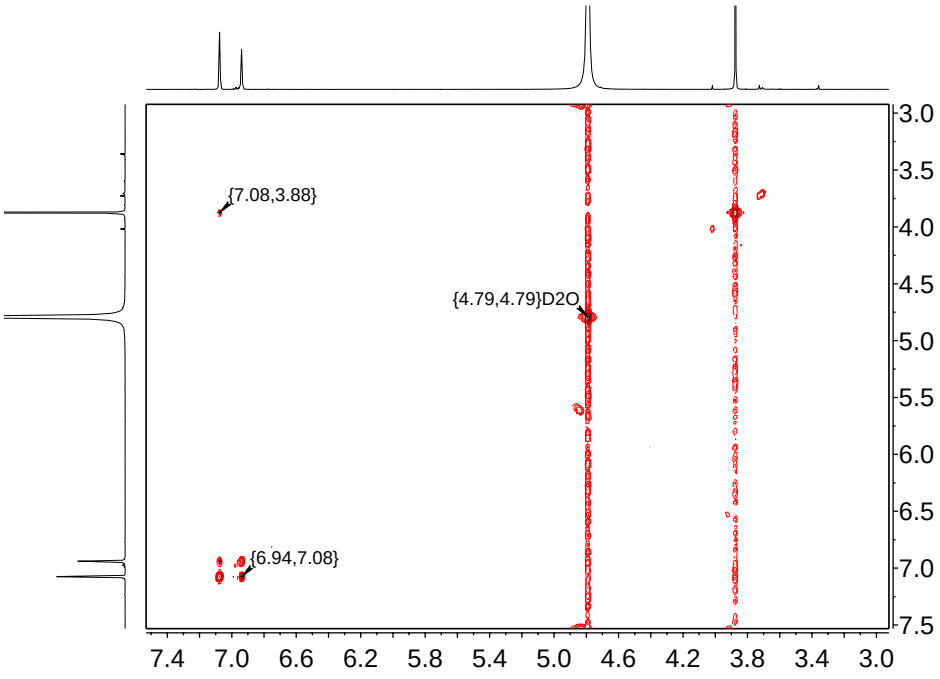

Figure S10. Full ^{1}H-^{1}H COSY spectrum of synthesized [4,6-D_2]-**I** [3.3 × 10^{-2} M] sample. The area plotted shows the ^{1}H spectrum in the range 7.5 to 3.0 ppm on both axes. The four-bond correlation is the same as depicted in Figure S9. Additionally, the five-bond ^{1}H-^{13}C(-3)-^{13}C(-2)-O-^{13}C(-7)-^{1}H correlation between the proton in position C-3 at 7.08 ppm and methoxy protons in position C-7 is observed.

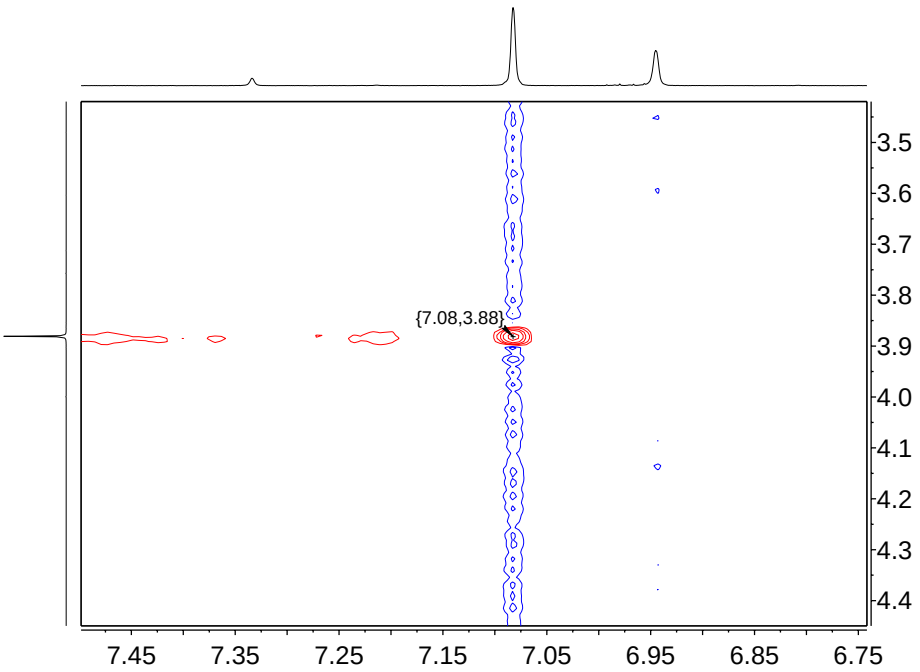

Figure S11. ^{1}H-^{1}H NOESY spectrum of synthesized [4,6-D_2]-**I** [3.3 × 10^{-2} M] sample depicting C-3/C-7 NOE correlation. The section plotted shows the ^{1}H spectrum in the range 7.47 to 6.75 ppm on the *x* axis and ^{1}H spectrum in the range 4.4 to 3.45 ppm on the *y* axis.

Table S1 below summarizes the ^{1}H and ^{13}C chemical shifts of guaiacol in positions C1-C7.

Table S1. Relative ^{1}H and ^{13}C resonances of guaiacol in positions C1-C7 (700 MHz, D_2O)

Position	^{1}H (ppm)	^{13}C (ppm)
C1	-	144
C2	-	147
C3	7.09	112.7
C4	6.99	121
C5	6.95	121.6
C6	6.97	115
C7	3.89	55.8

S3. Full ^{1}H and ^{13}C-NMR spectra of pure guaiacol in D_2O and homogeneous H/D exchanged guaiacol after reaction in D_2O at 423 K

Figures S12a and S12b show the $^{13}C\{^{1}H\}$ NMR spectra (126 MHz, D_2O, chemical shift from 20-180 ppm) of **I** (before homogeneous exchange, in D_2O) and the resulting solution after homogeneous exchange (24 h of **I**-D_2O-He reaction at 473 K, without the Ru catalyst), respectively. The truncated ^{13}C-NMR spectra are shown in Figure 1b of the main manuscript.

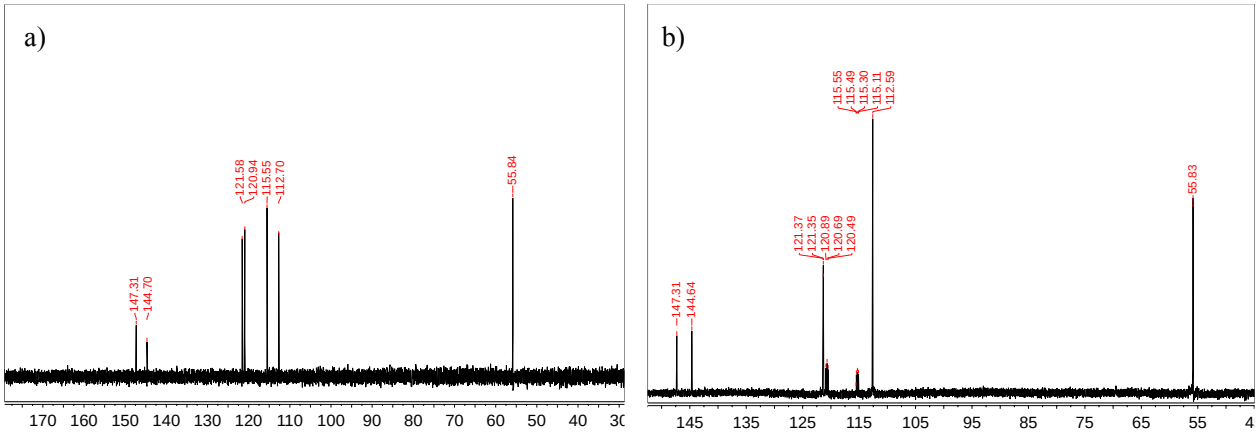

Figure S12. ^{13}C NMR (126 MHz, D_2O) of a) pure guaiacol (**I**) in D_2O and b) the resulting solution after homogeneous exchange (24 h of **I**-D_2O-He reaction at 473 K, 4.1 × 10^{-2} M of **I** and 10 bar He).

Figures S13a and S13b show the ^{1}H-NMR spectra of **I** (before homogeneous exchange, in D_2O) and the resulting solution after homogeneous exchange (24 h of **I**-D_2O-He reaction at 473 K), respectively. The truncated ^{1}H-NMR spectra are shown in Figure 1c of the main manuscript.

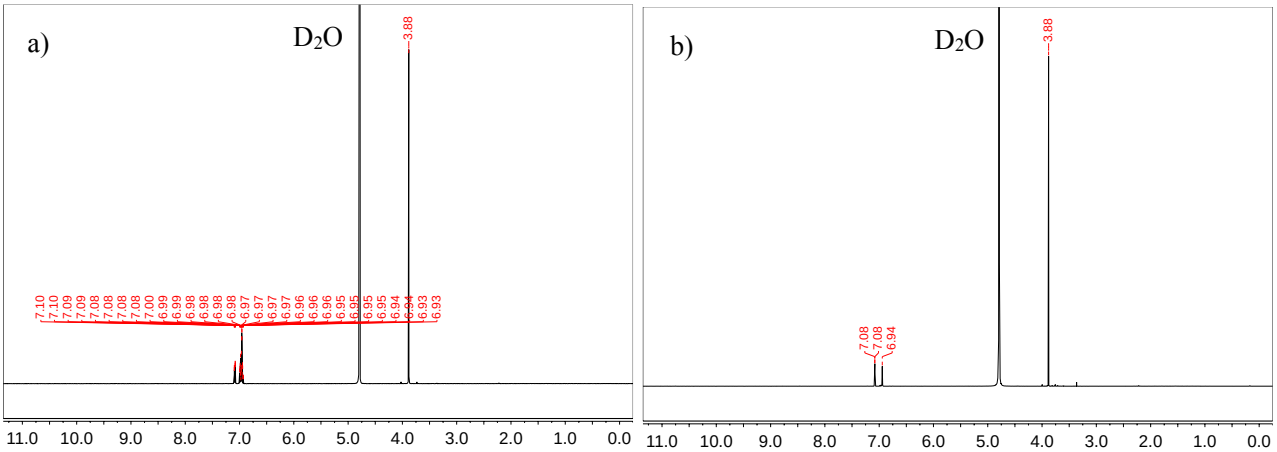

Figure S13. ^{1}H NMR spectra (500 MHz, 25 °C, D_2O) of a) pure guaiacol (**I**) and b) quantitative ^{1}H NMR spectra (600 MHz, 25 °C, D_2O) homogeneous exchange sample (qNMR parameters: number of scans = 64, relaxation delay = 60, pulse width = 10.2, acquisition time = 4).

S4. Derivation of $k_{\text{C-6}}^{\text{H}^+}$ and $k_{\text{C-4}}^{\text{H}^+}$ values using Brønsted-Evans-Polanyi relation and Marcus expressions

The acid-catalyzed rate constants of phenolic compound to form its keto isomer, i.e., $k_{\text{C-}a1}^{\text{H}^+}$ (step L^+, C-*a1* of Scheme 2 of the main manuscript), follow the Brønsted-Evans-Polanyi (BEP) relation[2-3] and Marcus expression:[4]

$$k_{\text{C-}a1}^{\text{H}^+} = k_{\text{diffusion}}^{\text{H}^+} \exp\left(\frac{-\Delta G^{\text{TS}}}{RT}\right) \tag{S6a}$$

where $$\Delta G^{\text{TS}} = \Delta G_0^{\text{TS}} \left(1 + \frac{\Delta G^0}{4\Delta G_0^{\text{TS}}}\right)^2 \tag{S6b}$$

$$\Delta G^0 = -2.3RT \cdot \text{p}K_{\text{a}}^{\text{keto,H}^+} \tag{S6c}$$

where $k_{\text{diffusion}}^{\text{H}^+}$ denotes the diffusional limit of H^+ in the aqueous phase from the "Eigen"-curve[5] and is assumed to be 3.6×10^{14} M^{-1} h^{-1} [3]; ΔG^{TS} and ΔG^0 denote the free energy of activation and the standard Gibbs free energy of proton addition onto enol anion (i.e., step H^+, C-*a1*, Scheme 2b of the main manuscript) at temperature *T*; ΔG_0^{TS} denotes the intrinsic Marcus barrier of a thermoneutral reaction (i.e., $\Delta G^0 = 0$) and has been regressed to be 57 kJ mol^{-1} for enol anions;[3] $K_{\text{a}}^{\text{keto,H}^+}$ denotes the acid-dissociation constant of a keto as a carbon-acid (i.e., $K_{\text{a}}^{[a1\text{-H}]\text{-}\mathbf{Ik},\text{H}^+}$ for the formed [*a1*-H]-**Ik** of step H^+, C-*a1*).

Because the net result of step acid-dissociation and step H^+, C-*a1* is the formation of [*a1*-H]-**Ik**, the $\text{p}K_{\text{a}}^{[a1\text{-H}]\text{-}\mathbf{Ik},\text{H}^+}$ can be estimated from:

$$\text{p}K_{\text{a}}^{[a1\text{-H}]\text{-}\mathbf{Ik},\text{H}^+} = \text{p}K_{\text{a}}^{\mathbf{I},\text{H}^+} - \text{p}K_{\text{isomerization}}^{\mathbf{I}\text{-to-}[a1\text{-H}]\text{-}\mathbf{Ik}} \tag{S7}$$

where $K_{\text{isomerization}}^{\mathbf{I}\text{-to-}[a1\text{-H}]\text{-}\mathbf{Ik}}$ denotes the enol-keto isomerization equilibrium constant of I to [*a1*-H]-**Ik** (i.e., reaction sum of step acid-dissociation and step H^+, C-*a1*, Scheme 2b of main manuscript). Due to the structural similarity between phenol and guaiacol, we estimate that the $K_{\text{isomerization}}^{\mathbf{I}\text{-to-[6-H]-}\mathbf{Ik}}$ and $K_{\text{isomerization}}^{\mathbf{I}\text{-to-[4-H]-}\mathbf{Ik}}$ from the equilibrium constant values for reactions involving phenol isomerization via H-transfer from a hydroxyl to ortho carbon (i.e., for phenol conversion to cyclohexa-2,5-dienone, $K_{\text{isomerization}}^{\text{phenol-to-cyclohexa-2,5-dienone}}$, of $10^{-12.73}$ at 298

K[6]) and para carbon atoms (i.e., for phenol conversion to cyclohexan-2,4-dienone, $K_{\text{isomerization}}^{\text{phenol-to-cyclohexa-2,4-dienone}}$, of $10^{-10.85}$ at 298 K[6]), respectively. Substituting the phenol isomerization equilibrium constant values, together with the reaction enthalpy (74.8 kJ mol^{-1} [6] and 61.9 kJ mol^{-1} [6] for phenol isomerization via H-transfer to ortho and para carbon atoms, respectively), into the van't Hoff Equation and assuming negligible reaction entropy (<3 J mol^{-1} K^{-1} [6]), gives the $pK_a^{[6\text{-H}]\text{-}\mathbf{Ik},H^+}$ and $pK_a^{[4\text{-H}]\text{-}\mathbf{Ik},H^+}$ values of 1.1 and -0.1, respectively, at 423 K. These $pK_a^{[6\text{-H}]\text{-}\mathbf{Ik},H^+}$ and $pK_a^{[4\text{-H}]\text{-}\mathbf{Ik},H^+}$ values, when substituting into Equations S6c, S6b, and S6a, give $k_{\text{C-6}}^{H^+}$ and $k_{\text{C-4}}^{H^+}$ values of 3.1×10^7 M^{-1} h^{-1} and 6.2×10^7 M^{-1} h^{-1}, respectively, at 423 K.

S5. Derivation of H/*L* exchange turnover rate ratio and turnover rate expression via Proton-Electron Transfer (PET) and *L** addition pathways

The theoretical turnover rate ratio for H/*L* exchange on *C-a1* (*a1* = 3 or 5) of **I** via Proton-Electron Transfer (PET) to that via *L** addition pathways (Scheme 3, Section 3.2 of the main manuscript) according to Equations 4a and 4b of the main manuscript, using an Eyring equation and free energy expressions, is

$$\frac{TOR_{\text{H-}L\text{ exchange, C-}a1}^{\text{PET}}}{TOR_{\text{H-}L\text{exchange, C-}a1}^{L^*\text{ addition}}} = \frac{k_{5,\text{ C-}a1}^{L^+} K_4^{L^*} K_{3,\text{ O-}L\text{ cleavage}}^{\mathbf{I}} K_1^{\mathbf{I}}}{\frac{k_{5,\text{ C-}a1}^{L^+}}{K_{5,\text{ C-}a1}^{L^+}} K_{7,\ L^*\text{ addition, C-}a1}^{\text{guaioxyl}} K_{3,\text{ O-}L\text{ cleavage}}^{\mathbf{I}} K_1^{\mathbf{I}}} = \exp\left(-\frac{\left(G_{\text{PET, C-}a1}^{\text{TS}} - G_{L^*\text{ addition, C-}a1}^{\text{TS}}\right)}{RT} \right) \quad \text{(S8a)}$$

where $G_{\text{PET, C-}a1}^{\text{TS}}$ and $G_{L^*\text{ addition, C-}a1}^{\text{TS}}$ are the transition state free energies of the forward (i.e., when evaluating from the PET direction) and the reverse (when evaluating from the *L** addition direction) reactions of step 5, respectively. From Equation S8a, the turnover rate ratio of H/*L* exchange via the PET pathway to that via the *L** addition pathway depends on the free energy difference of their transition state via these two pathways.

The diagrams (showing only C-*a1* for simplicity) in Scheme 4c describe how the transition states for C-*L* bond formation and rupture differ from one another. The $G_{\text{PET, C-}a1}^{\text{TS}}$ and $G_{L^*\text{ addition, C-}a1}^{\text{TS}}$ values are identical (reaction coordinates in Scheme 4a) to each other only in H_2O-H_2 (*L* = H, as shown in Scheme 4a) but not in D_2O-D_2 (when *L* = D in Scheme 4a) because the difference in their transition state structure as depicted in Scheme 4c.

The difference between the PET and *L** addition arises solely from the fact that the former occurs via L^+ added from above the ring and the latter via *L** addition from below the ring. Thus, $G^{\mathrm{TS}}_{\mathrm{PET,\ C\text{-}}a1}$ must remain similar to $G^{\mathrm{TS}}_{L^*\ \mathrm{addition,\ C\text{-}}a1}$ either in H_2O-H_2 or in D_2O-D_2 (i.e., $G^{\mathrm{TS}}_{\mathrm{PET,\ C\text{-}}a1} - G^{\mathrm{TS}}_{L^*\ \mathrm{addition,\ C\text{-}}a1} \approx 0$ kJ mol^{-1}), leading to a nearly identical and indistinguishable H/*L* exchange rate for both pathways:

$$\frac{TOR^{\mathrm{PET}}_{\mathrm{H}\text{-}L\ \mathrm{exchange,\ C}\text{-}a1}}{TOR^{L^*\ \mathrm{addition}}_{\mathrm{H}\text{-}L\mathrm{exchange,\ C}\text{-}a1}} \approx 1 \tag{S8b}$$

Because guaioxyl-χ* covers the Ru surface and adsorbs on χ number of Ru surface atoms,[1] θ_* is

$$\theta_* = \frac{1}{\chi \cdot \frac{K^{\mathbf{I}}_{3,\ \mathrm{O}\text{-}L\ \mathrm{cleavage}} K^{\mathbf{I}}_1 [\mathbf{I}]}{\left(K_2^{L_2} P_{L_2}\right)^{0.5}} \theta_*^{\chi-1}} \tag{S9}$$

where the denominator in Equation S9 denotes the coverage ratio between guaioxyl-χ* and empty sites on the surface (*). Substituting Equation S9 into Equation 4a (numerically identical to substituting into Eq. 4b) leads to

$$TOR^{\mathrm{PET}}_{\mathrm{H}\text{-}L\ \mathrm{exchange,\ C}\text{-}a1} = \chi^{-1} k^{L^+}_{5,\ \mathrm{C}\text{-}a1} K_4^{L^*} \left(a_{\mathbf{I}}\right)^0 \left(K_2^{L_2} \, f_{L_2} \Big/ f^0 \right)^{0.5} \tag{S10a}$$

Equation S10a predicts that the reaction order of the H/*L* exchange is 0 and 0.5 with respect to the concentration of **I** and the H_2 pressure (P_{L_2}), respectively. In D_2O-D_2 (*L* = D), Equation S10a becomes

$$TOR^{\mathrm{PET}}_{\mathrm{H\text{-}D\ exchange,\ C}\text{-}a1} = \chi^{-1} k^{\mathrm{D}^+}_{5,\ \mathrm{C}\text{-}a1} K_4^{\mathrm{D}^*} \left(a_{\mathbf{I}}\right)^0 \left(K_2^{D_2} \, f_{D_2} \Big/ f^0 \right)^{0.5} \tag{S10b}$$

S6. Free energy profiles of guaiacol HDO and hydrogenation elementary steps via initial H* addition on C-3

Scheme S1 shows the free energy profile counterparts for Scheme 5 of the main manuscript, where initial H* addition occurs on C-3.

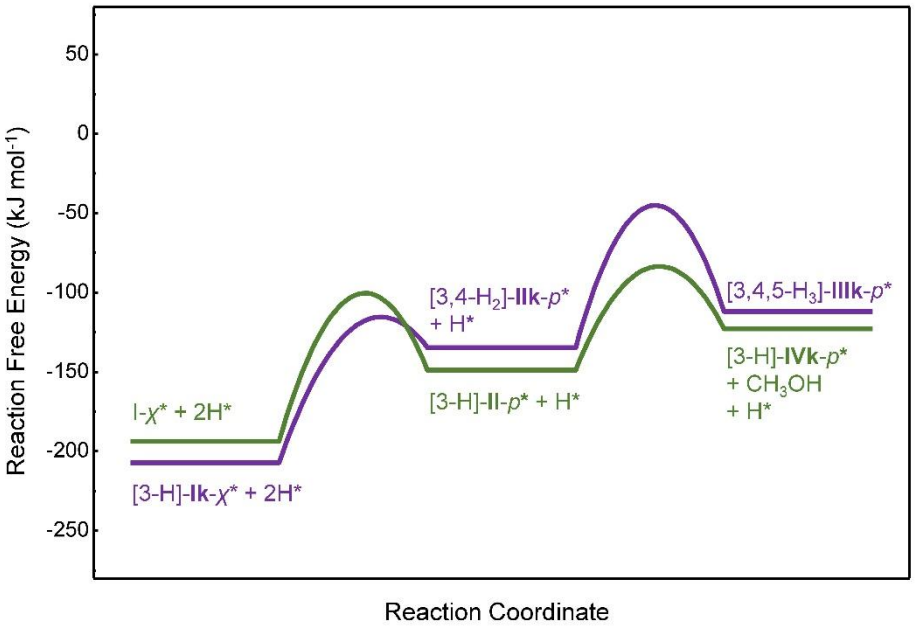

Scheme S1. Gibbs reaction energy profile for the guaiacol (**I**) HDO and hydrogenation elementary steps at 423 K at the Ru-H_2O interface in H_2 when the initial quasi-equilibrated H* addition occurs on C-*a1* (*a1* = 3). The ***L*-addition route** (denoted with purple) proceeds via a quasi-equilibrated H* addition onto [3-H]-**Ik**-χ* (step 8) followed by the rate limiting H* addition onto [3,4-L_2]-**IIk**-*p** (step 9), whereas the **C-OCH_3 cleavage route** (denoted with green) proceeds via a quasi-equilibrated H* addition onto the **I**-χ* species (step 10) followed by the rate limiting, concerted intramolecular proton transfer and C-OCH_3 bond cleavage of the [*a1*-*L*]-**II**-*p** intermediate (step 11).

S7. Ruling out C-OCH$_3$ bond cleavage of I-χ* via intramolecular proton transfer

We consider and then rule out the possibility of adsorbed guaiacol (**I**-χ*) to undergo direct C-OCH$_3$ rupture via an initial intramolecular transfer from its hydroxyl group:

step S1 $$C_6H_4(OH)(OCH_3)-\chi^* \leftrightarrows C_6H_4(O)-\chi^*+CH_3OH$$

By comparing the rate of the above reaction, $r_{\text{C-O,S1}}$, with that of the direct H* addition, $r_{\text{H-addition,10}}$ (shown as step 10 in Scheme 5a), we can derive the rate ratio of C-O bond rupture via intramolecular proton transfer of adsorbed guaiacol to H* addition:

$$\frac{r_{\text{C-O,S1}}}{r_{\text{H-addition,10}}} = \frac{k_{\text{S1}}}{k_{10}\sqrt{K_2 \, f_{\text{H}_2} / f^0}} \quad \text{(S11)}$$

where k_{S1} and k_{10} denote the rate constants of steps S1 and 10, respectively. At 423 K and the moderate coverage of 0.083 ML guaiacol (58% of saturation) and 0.167 ML H* (17% of saturation) modeled with DFT calculations, the activation free energy of step S1 is 82 kJ mol^{-1}. The H-addition step onto C-3 or C-5 of **I**-χ* exhibit activation free energies of 93 and 94 kJ mol^{-1}, respectively, and H_2 adsorption is exergonic by ~-44 kJ mol^{-1}. Substituting these values into Equation S11 leads to a rate ratio of only 0.04 at 1 bar of H_2 pressure. Thus, step S1 must be kinetically unfavorable compared with direct H-addition at higher H_2 pressure in the typical experimental conditions (10-50 bar).

We can also consider the kinetic consequences of intramolecular C-OCH$_3$ bond rupture to occur prior to any H-addition from an experimental perspective. In this mechanistic case, the subsequent H-addition event(s) must be rate-limiting as imposed by the measured, close-to-unity H_2 dependence of the C-OCH$_3$ bond cleavage route. In such a scenario, the C-OCH$_3$ bond rupture must be reversible. A reversible C-OCH$_3$ bond rupture via intramolecular proton transfer in a polar protic water solvent will ultimately lead to solvolysis, as shown in steps S2 and S3:

step S2 $$C_6H_4(O)-\chi^*+H_2O \leftrightarrows C_6H_4(OH)(OH)-\chi^*$$

step S3 $$C_6H_4(OH)(OCH_3)-\chi^*+H_2O \leftrightarrows C_6H_4(OH)(OH)-\chi^*$$

where step S2 can be thought to be the reversed reaction of step S1, but water, instead of methanol, attacks the surface $C_6H_4(O)$ fragment. Step S3 is the lumped total of solvolysis reaction. If this is the case, one would observe the formation of catechol (i.e., $C_6H_4(OH)(OH)$) in excess water in the absence of H_2, and the catechol formation rate must be greater than the C-OCH_3 bond rupture rate. Throughout our previous[1] and current kinetic isotopic measurements, catechol and its derivatives (i.e., cyclohexadiol) remain largely undetectable. Therefore, the solvolysis must be kinetically inconsequential and the C-OCH_3 bond rupture cannot be reversible (i.e., steps S1 and S2 do not occur).

In conclusion, the mechanistic proposal of C-OCH_3 bond rupture prior to H* addition contradicts the density functional theory results (i.e., much smaller effective barrier of step S1 vs. step 10), kinetic evidence (i.e., first-order H_2 dependence for C-OCH_3 bond rupture route), and measured product distributions (i.e., absence of catechol derived intermediates[1]). Based on these results, we rule out the initial C-OCH_3 bond cleavage of adsorbed guaiacol (**I-**χ*), either via direct metal insertion or intramolecular proton transfer, as the prevalent pathway.

S8. Ruling out C-OCH_3 bond cleavage via direct metal oxidative addition

Adjacent vacant Ru site (i.e., *) may assist with the metal oxidative addition of [*a1-L*]-**II**-*p** or [*a1*,4-L_2]-**IIk**-*p** to cleave their C-OCH_3 bond in an irreversible step, as shown in steps S4 (with a rate constant k_{S4}) and S5 (with a rate constant k_{S5}), respectively:

step S4 $$[a1\text{-}L]\text{-}\mathbf{II}\text{-}p^* + * \longrightarrow [a1\text{-}L]\text{-}\mathbf{V}\text{-}p^* + CH_3O^*$$

step S5 $$[a1,4\text{-}L_2]\text{-}\mathbf{IIk}\text{-}p^* + * \longrightarrow [a1,4\text{-}L_2]\text{-}\mathbf{Vk}\text{-}p^* + CH_3O^*$$

Assuming that these steps limit the guaiacol conversion via **C-OCH$_3$** bond cleavage route, the turnover rate expression of **C-OCH$_3$** bond cleavage route via step S4 or S5 as the rate-limiting step ($TOR^{Sx}_{\text{C-OCH}_3\text{ cleavage, }L}$, x = 4 or 5) at conditions when guaioxyl-χ* is the MASI[1] is given by Equation S12a or S12b, respectively:

$$TOR^{S4}_{\text{C-OCH}_3\text{ cleavage, }L} = k_{S4} K_1^{\mathbf{I}} \left(K_2^{L_2}\right)^{0.5} K^{\mathbf{I}}_{11,\, L^*\text{ addition}} \cdot [\mathbf{I}] \cdot \left(f_{L_2} \Big/ f^0 \right)^{0.5} \cdot \theta_*^{\,p+1} \quad \text{(S12a)}$$

$$TOR^{S5}_{\text{C-OCH}_3\text{ cleavage, }L} = k_{S5} K_1^{\mathbf{I}} \left(K_2^{L_2}\right)^{0.5} K^{\mathbf{I}}_{3,\,\text{O-}L\text{ cleavage}} K^{\text{guaioxyl}}_{7,\,L^*\text{ addition}} K^{[a1-L\text{-}\mathbf{Ik}]}_{8,\,L^*\text{ addition}} \cdot [\mathbf{I}] \cdot \left(f_{L_2} \Big/ f^0 \right)^{0.5} \cdot \theta_*^{\,p+1} \quad \text{(S12b)}$$

These expressions and the proposed proton-electron transfer pathway exhibit identical kinetic dependences on **I**, L_2, and vacant Ru site (Eq. S14a), thus they are indistinguishable based merely on rate measurements. DFT calculations, however, have shown that the overall activation free energies, calculated based on Equation 3 of the main manuscript, would increase by at least 22 kJ mol^{-1} if either step S4 or S5, instead of step 11 (Scheme 4 of the main manuscript), are instead the kinetically relevant step. Based on the much larger activation free energies for these alternative steps, we thus rule out the kinetic relevance of direct C-OCH$_3$ bond cleavage via direct metal oxidative insertion.

S9. Ruling out the *L*-adatom addition of [*a1-L*]-II-*p** as the kinetically relevant step of the H-addition route

In competition to the intramolecular proton transfer, [*a1-L*]-**II**-*p** can also undergo a subsequent, kinetically relevant *L** addition on its ring, as shown in step S6 (rate constant of k_{S6})

step S6 $$[a1\text{-}L]\text{-}\mathbf{II}\text{-}p^* + L^* \longrightarrow [a1,a2\text{-}L_2]\text{-}\mathbf{III}\text{-}p^* + *$$

This was proposed previously, based on kinetic measurements, to be the kinetically relevant step of this route. [1] If step S6 limits the guaiacol conversion via ***L*-addition** route, the turnover rate expression for ***L*-addition** route ($TOR^{S6}_{L-\text{addition}}$) at conditions when guaioxyl-χ* is the MASI [1], is

$$TOR^{S6}_{L-\text{addition}} = k_{S6} K_1^{\mathbf{I}} K_2^{L_2} K_{11,\,L^*\,\text{addition}}^{\mathbf{I}} \cdot [\mathbf{I}] \cdot f_{L_2} \cdot \theta_*^{\,p+1} \quad \text{(S13)}$$

When considering the turnover expression of the proposed rate-limiting step in this study (i.e., Eq. S14a), both proposed pathways give identical **I**, L_2, and vacant Ru site dependences. Next, we examine and rule out this alternative route hereby using DFT calculations. [*a1-L*]-**II**-*p** undergoes subsequent H* addition, most favorably on C-*a2* (*a2* = 3 or 5, *a2* ≠ *a1*), with activation free energies of 109 kJ mol^{-1} (*a1* = 3) and 89 kJ mol^{-1} (*a1* = 5). The overall, effective activation free energies of H* addition onto [3-*L*]-**II**-*p** and [5-*L*]-**II**-*p** are 12 and 21 kJ mol^{-1} higher than their corresponding intramolecular proton transfer (step 11), respectively. At 423 K, the effective activation barrier difference leads the intramolecular proton transfer to occur >4 times faster even at 50 bar H_2 (Supporting Information), indicating that most of the [*a1-L*]-**II**-*p** undergoes C-OCH_3 bond rupture instead of further H* addition. We thus rule out the kinetic relevance of *L** addition to [*a1-L*]-**II**-*p** intermediate during **I**-H_2-H_2O reaction on Ru clusters.

S10. Derivation of Equations 6a-6d of the main manuscript

From the proposed mechanisms in Scheme 4, the turnover rates of the ***L*-addition** ($TOR_{L-\text{addition}}$) and **C-O** bond cleavage ($TOR_{\text{C-OCH}_3\text{ cleavage, }L}$) routes are

$$TOR_{L-\text{addition}} = k_{9,\,L^*\text{ addition}}^{[a1,4-L_2\text{-IIk}]} K_1^{\mathbf{I}} K_2^{L_2} K_{3,\,\text{O-}L\text{ cleavage}}^{\mathbf{I}} K_{7,\,L^*\text{ addition}}^{\text{guaioxyl}} K_{8,\,L^*\text{ addition}}^{[a1-L\text{-Ik}]} \cdot [\mathbf{I}] \cdot \left(f_{L_2} \Big/ f^0 \right) \cdot \theta_*^{\,p+1} \tag{S14a}$$

$$TOR_{\text{C-OCH}_3\text{ cleavage, }L} = k_{12,\,L^+}^{[a1\text{-}L\text{-II}]} K_1^{\mathbf{I}} \left(K_2^{L_2} \right)^{0.5} K_{11,\,L^*\text{ addition}}^{\mathbf{I}} \cdot [\mathbf{I}] \cdot \left(f_{L_2} \Big/ f^0 \right)^{0.5} \cdot \theta_*^{\,p+1} \tag{S14b}$$

The rate and equilibrium constants are defined in Schemes 4 and 5 of the main manuscript. Since guaioxyl-χ* is the MASI,[1] substituting Equation S9 into Equations S14a and S14b gives

$$TOR_{L-\text{addition}} = k_{L-\text{addition}}^{\text{eff}} \left([\mathbf{I}] \right)^{1-\frac{p+1}{\chi}} \left(f_{L_2} \Big/ f^0 \right)^{1+\frac{p+1}{2\chi}} \tag{S15a}$$

$$TOR_{\text{C-OCH}_3\text{ cleavage, }L} = k_{\text{C-OCH}_3,\,L}^{\text{eff}} \left([\mathbf{I}] \right)^{1-\frac{p+1}{\chi}} \left(f_{L_2} \Big/ f^0 \right)^{0.5+\frac{p+1}{2\chi}} \tag{S15b}$$

where $k_{L-\text{addition}}^{\text{eff}} = (\chi)^{-\frac{p+1}{\chi}} k_{9,\,L^*\text{ addition}}^{[a1,4-L_2\text{-IIk}]} \left(K_1^{\mathbf{I}} K_{3,\,\text{O-}L\text{ cleavage}}^{\mathbf{I}} \right)^{1-\frac{p+1}{\chi}} \left(K_2^{L_2} \right)^{1+\frac{p+1}{2\chi}} K_{7,\,L^*\text{ addition}}^{\text{guaioxyl}} K_{8,\,L^*\text{ addition}}^{[a1-L\text{-Ik}]}$ (S15c)

$$k_{\text{C-OCH}_3\text{ cleavage, }L}^{\text{eff}} = (\chi)^{-\frac{p+1}{\chi}} k_{12,\,L^+}^{[a1\text{-}L\text{-II}]} \left(K_1^{\mathbf{I}} \right)^{1-\frac{p+1}{\chi}} \left(K_2^{L_2} \right)^{0.5+\frac{p+1}{2\chi}} \left(K_{3,\,\text{O-}L\text{ cleavage}}^{\mathbf{I}} \right)^{-\frac{p+1}{\chi}} K_{11,\,L^*\text{ addition}}^{\mathbf{I}} \tag{S15d}$$

Equations S15a-S15d appear as Equations 6a-6d of the main manuscript.

S11. Derivation of DFT-based effective kinetic isotope effects for the routes involving *L*-addition and C-OCH_3 bond cleavage

Substituting Equations 6a-6b and 8a-8b into Equations 9a and 9b leads to

$$KIE^{\mathrm{DFT}}_{L-\text{addition, C-}a1} = KIE^{[a1,4-\mathrm{H_2}\text{-}\mathbf{IIk}]}_{9,\ L^*\text{ addition}} \left(EIE_2^{L_2}\right)^{1-\frac{p+1}{2\chi}} \left(EIE^{\mathbf{I}}_{3,\ \text{O-}L\text{ cleavage}}\right)^{1-\frac{p+1}{\chi}} EIE^{\text{guaioxyl}}_{7,\ L^*\text{ addition}} EIE^{[a1-\text{H-}\mathbf{Ik}]}_{8,\ L^*\text{ addition}} \quad \text{(S16a)}$$

$$KIE^{\mathrm{DFT}}_{\text{C-OCH}_3\text{ cleavage, }L\text{, C-}a1} = KIE^{[a1\text{-}L\text{-}\mathbf{II}]}_{12,\ L^+} \left(EIE_2^{L_2}\right)^{0.5-\frac{p+1}{2\chi}} \left(EIE^{\mathbf{I}}_{3,\ \text{O-}L\text{ cleavage}}\right)^{-\frac{p+1}{\chi}} EIE^{\mathbf{I}}_{11,\ L^*\text{ addition,}} \quad \text{(S16b)}$$

Substituting DFT-derived KIE_j and EIE_j values in this study (Schemes 3 and 4) and a $(p+1)\chi^{-1}$ value of 0.78 ± 0.2 based on previous kinetic measurement and rate regressions[1] into Equations S16a and S16b leads to the $KIE^{\mathrm{DFT}}_{L-\text{addition, C-3}}$ and $KIE^{\mathrm{DFT}}_{\text{C-OCH}_3\text{ cleavage, }L\text{, C-3}}$ values of 0.50 and 0.24, respectively, and the $KIE^{\mathrm{DFT}}_{L-\text{addition, C-5}}$ and $KIE^{\mathrm{DFT}}_{\text{C-OCH}_3\text{ cleavage, }L\text{, C-5}}$ values of 0.44 and 0.23, respectively.

References:

1. Shangguan, J.; Pfriem, N.; Chin, Y.-H. C., Mechanistic details of CO bond activation in and H-addition to guaiacol at water-Ru cluster interfaces. *J. Catal.* **2019,** *370*, 186-199.
2. Chiang, Y.; Kresge, A. J.; Santaballa, J.; Wirz, J., Ketonization of acetophenone enol in aqueous buffer solutions. Rate-equilibrium relations and mechanism of the uncatalyzed reaction. *J. Am. Chem. Soc.* **1988,** *110*, 5506-5510.
3. Wirz, J., Kinetics of proton transfer reactions involving carbon. *Pure Appl. Chem.* **1998,** *70*, 2221-2232.
4. Marcus, R. A., Theoretical relations among rate constants, barriers, and Brønsted slopes of chemical reactions. *The Journal of Physical Chemistry* **1968,** *72*, 891-899.
5. Eigen, M., Proton Transfer, Acid□Base Catalysis, and Enzymatic Hydrolysis. Part I: Elementary Processes. *Angew. Chem. Int. Ed.* **1964,** *3*, 1-19.
6. Capponi, M.; Gut, I. G.; Hellrung, B.; Persy, G.; Wirz, J., Ketonization equilibria of phenol in aqueous solution. *Can. J. Chem.* **1999,** *77*, 605-613.